



Enhanced performance of amine and thiol chemically modified graphene oxide for effective removal of Hg(II), Pb(II), and Cr(VI) from aqueous solution

Ayyob M. Bakry¹ · Waleed M. Alamier¹ · A. B. Abdallah^{2,3} · Yasmeen G. Abou El-Reash⁴ · M. Samy El-Shall⁵ · Fathi S. Awad^{2,3}

Received: 14 February 2024 / Accepted: 25 June 2024 / Published online: 23 July 2024
© The Author(s) 2024

Abstract

This study describes a novel adsorbent with a multidentate ligand that was facilely fabricated by covalently bonding 4-amino-3-hydrazino-5-mercapto-1,2,4-triazole on graphene oxide (AHMT-PRGO). The AHMT-PRGO nano-adsorbent was used for the effective removal of Hg(II), Pb(II), and Cr(VI) from wastewater. The AHMT-PRGO nano-adsorbent was synthesized by a nucleophilic substitution reaction between GO acyl chloride and AHMT chelating ligand in the presence of tetrabutylammonium bromide as a catalyst. The successful modifications were confirmed via several spectroscopic and electron microscopy instrumentations including UV–Vis, FTIR, Raman, XRD, XPS, SEM, and TEM. The maximum adsorption capacities of Hg(II), Cr(VI), and Pb(II) on the AHMT-PRGO nano-adsorbent were 370.0, 136.2, and 109.6 mg/g, respectively, exceeding those of most previously reported adsorbents. Additionally, the equilibrium contact times for Hg(II), Pb(II), and Cr(VI) were 60, 30, and 400 min, respectively. In a mixture of nine heavy metal ions containing 250 ppm of each ion, the AHMT-PRGO nano-adsorbent exhibited high selectivity for Hg(II) ions. Furthermore, the AHMT-PRGO nano-adsorbent showed high stability over five adsorption–desorption cycles. Additionally, the AHMT-PRGO nano-adsorbent was successfully applied to remove heavy metal ions from real water samples. The novelty of AHMT-PRGO lies in the combination of a multidentate ligand for strong and selective binding with the high surface area and stability offered by covalently bonded graphene oxide. This combination offers potential advantages over traditional adsorbents in terms of adsorption capacity, selectivity, and reusability.

Keywords AHMT-PRGO · Graphene oxide · Adsorption · Pb(II) · Cr(VI) · Hg(II)

Introduction

Water is essential for all life on Earth. Unfortunately, human activity, including industrialization and population growth, has significantly reduced water quality. This pollution comes from various sources, including radioactive materials, chemicals, and harmful microorganisms. One major type of water pollutant is heavy metals. These elements, like mercury, lead, and arsenic, are denser than water and very toxic. Industries often discharge them as waste without proper treatment, contaminating freshwater sources. These metal ions are persistent and enter the food chain, posing a serious threat to human health and the environment. Heavy metal poisoning can cause severe and chronic diseases. Examples include organ damage, respiratory problems, anemia, bone issues, cancer, and high blood pressure. Therefore, finding ways to remove these toxic metals from polluted water is

✉ Fathi S. Awad
fathyawad949@yahoo.com; fathysamy@mans.edu.eg

¹ Department of Physical Sciences, Chemistry Division, College of Science, Jazan University, P.O. Box 114, 45142 Jazan, Saudi Arabia

² Chemistry Department, Faculty of Science, Mansoura University, Mansoura 35516, Egypt

³ Chemistry Department, Faculty of Science, New Mansoura University, New Mansoura City, Egypt

⁴ Department of Chemistry, College of Science, Imam Mohamed Ibn Saud Islamic University (IMSIU), P.O. Box, 90950, 11623 Riyadh, Saudi Arabia

⁵ Department of Chemistry, Virginia Commonwealth University, Richmond, VA 23284, USA

crucial (Awual 2019; Richardson and Ternes 2022; Vardhan et al. 2019).

There are many ways to remove heavy metals from polluted water. These include ion exchange, chemical precipitation, and filtration methods like reverse osmosis and membranes. Other options are solvent extraction and electrochemical treatment (Awual et al. 2017; Sathya et al. 2022; Sharma and Bhattacharya 2017; Sikosana et al. 2019). Adsorption is a particularly effective technique for cleaning industrial wastewater from heavy metals. It's relatively simple, cost-effective, and reusable, with the ability to target specific metals. During adsorption, metal ions in the water are attracted to the surface of an adsorbent material through physical or chemical interactions. This process results in high-quality treated water. Adsorption offers several advantages over other methods. First, the captured metal ions can be desorbed using appropriate solutions, allowing the adsorbent to be reused and minimizing waste. Second, the adsorbent can be tailored to extract specific metals even in the presence of others, which is crucial for industrial applications with mixed metal contamination (Bakry et al. 2020a, b, c; Bakry et al. 2022; Yu et al. 2020). In recent years, widespread materials have been studied as adsorbents for heavy metal removal (Awual et al. 2024; Sheikh et al. 2023). Some of the most promising materials include inorganic nanomaterials (Ali et al. 2023; Bakry et al. 2020a, b, c) activated carbon (Sultana et al. 2022; Vedenyapina et al. 2021) nitrogen-doped porous carbons (Bakry et al. 2020a, b, c; Huang et al. 2023) porous silica (Awual 2017; Awual et al. 2023; Salman et al. 2023), covalent organic frameworks (da Silva et al. 2023; Gendy et al. 2021), zeolites (Velarde et al. 2023), metal-organic frameworks (Awad et al. 2021a, b; Lam et al. 2023), chitosan-based composit (Rehan et al. 2023), mesoporous silica (Grozdoz and Zinicovscaia 2023; Yang et al. 2023), and graphene oxide (Adel et al. 2022; Asghar et al. 2022).

There is a growing need for affordable and effective ways to remove harmful metals from wastewater. Graphene oxide (GO) is a promising material for this purpose because of its unique structure, stability, and large surface area. Scientists can modify GO with various ligands to capture metal ions from water (Bakry et al. 2020a, b, c; Bakry et al. 2022). Many GO-based adsorbents have been developed and demonstrated high removal efficiencies with fast kinetics and reusability. For example, MT-PRGO (Bakry et al. 2020a, b, c), Ca-Alginate-GO (Al-wakeel et al. 2022), CeO₂-PRGO (Bakry et al. 2022), IT-PRGO (Awad et al. 2017), DHAQ-GO (Khazaei et al. 2018), Mag-PRGO (Bobb et al. 2020), Melamine sponge rapped GO (Feng et al. 2019), PAN-PRGO (Awad et al. 2021a, b), AgNPs-GO (Vicente-Martínez et al. 2020), and Imino-IGO (Awad et al. 2018) have been successfully used to treat polluted water from a variety of heavy metals. The high performance of these GO-based

adsorbents is attributed to the following factors (Alzharani et al. 2022; Awad et al. 2021a, b; Bakry et al. 2022): firstly, the high surface area of GO produces plenty active sites for heavy metal adsorption. Secondly, the oxygen functional groups on GO nanosheets can react to poisonous metal ions via electrostatic and ion exchange interactions. Finally, the chelating ligands functionalized on GO can form strong coordination complexes with toxic metal ions. Therefore, GO-based adsorbents are a promising class of materials for heavy metal elimination from wastewater owing to their low cost, excellent performance, and ease of preparation.

This study introduces a brand new adsorbent, AHMT-PRGO, designed specifically to remove harmful metals like mercury, lead, and chromium from water. The adsorbent AHMT-PRGO was created by attaching a powerful chelating agent, 4-amino-3-hydrazino-5-mercapto-1,2,4-triazole (AHMT), to the surface of specially treated graphene oxide (CMGO) through a three-step process. First, graphene oxide (GO) nanosheets was obtained by oxidizing graphite. Then, the GO was chemically reacted with chloroacetic acid in a basic environment to create carboxylated GO (GO-COOH) with more carboxylic acid groups on its surface. Finally, GO-COOH was transformed into GO acyl chloride (GO-COCl) using thionyl chloride. The final step involved an amidation reaction between GO-COCl and the amine groups on the AHMT chelating agent, resulting in the novel AHMT-PRGO adsorbent. This unique, simple, and affordable method for producing AHMT-decorated GO-based adsorbent is entirely new. Initial tests show that AHMT-PRGO is highly effective at adsorbing metals, with fast kinetics and the ability to remove trace amounts of toxic metals from water. These promising results suggest that AHMT-PRGO has great potential for use in water treatment to remove harmful heavy metals.

Experimental section

Materials

All chemicals employed in this investigation were of analytical grade, as supplied by Sigma-Aldrich, and were utilized without further purification. Graphite powder (99.999%), 4-Amino-3-Hydrazino-5-Mercapto-1,2,4-Triazole (AHMT) (99%), Phosphoric acid (99%), Nitric acid (99%), Sulfuric acid (99%), Dimethylformamide (DMF) (99.99%), Potassium permanganate (99%), Tetrabutylammonium bromide (TBAB) (99%), Thionyl chloride (99%), Hydrogen peroxide (30%), and Ethanol (99%). HgCl₂, Pb(NO₃)₂, CdCl₂, Co(NO₃)₂·6H₂O, K₂Cr₂O₇, Ni(NO₃)₂·6H₂O, KH₂AsO₄, Zn(NO₃)₂·6H₂O, and CuCl₂·2H₂O, were dissolved in deionized water (DIW) to create various concentrations of individual metal ion stock solutions. These served as the source

for Hg(II), Pb(II), Cd(II), Co(II), Cr(VI), Ni(II), As(V), Zn(II), and Cu(II) ions, respectively.

Synthesis of the GO, GO-COOH and GO-COCl

Modified Hummer's method was employed to prepare GO with high surface area and oxygen functional groups (Awad et al. 2017; ; Bakry et al. 2020a, b, c). The surface density of carboxylic acid groups on GO was enhanced by dispersing (250 mg) GO in (250 mL) DIW and sonicating for 1 h. Subsequently, (5 g) Cl-CH₂COOH and (6 g) NaOH were added to the suspension and reacted for 3 h. The resulting product (GO-COOH) was neutralized to pH 6.5 with HNO₃, washed with DIW and C₂H₅OH, and dried at 60 °C for 12 h. Then (250 mg) of obtained GO-COOH was dispersed in (5 mL) of anhydrous DMF and sonicated for 60 min. Then, (40 mL) SOCl₂ was added, and the mixture was heated at 80 °C for 72 h. The final product (GO-COCl) was separated by centrifugation, washed with anhydrous DMF, and dried under vacuum.

Synthesis of AHMT-PRGO

(500 mg) GO-COCl was first dispersed in (10 mL) DMF by sonication for 2 h. Separately, (2 g) AHMT and (0.2 g) TBAB were dissolved in (20 mL) anhydrous DMF. Subsequently, the GO-COCl dispersion was added to the AHMT/TBAB solution in a three-necked round-bottom flask. The mixture was stirred at 25 °C for 2 h, followed by overnight reflux under a nitrogen atmosphere at 70 °C. The desired AHMT-PRGO product was isolated by centrifugation, thoroughly washed with DIW and C₂H₅OH and, and dried at 70 °C for 24 h.

Instrumentations

The GO, GO-COOH, GO-COCl, and AHMT-PRGO were characterized using a diversity of analytical techniques. Fourier transform infrared (FTIR) spectra were recorded using a Nicolet-Nexus 670 spectrometer equipped with a diamond ATR accessory. The measurement employed a resolution of 4 cm⁻¹ and 32 scans. Raman spectroscopy: A Thermo Scientific DXR Smart Raman spectrometer with 532 nm excitation was used to record the Raman spectra. Ultraviolet–visible (UV–VIS) spectra were recorded using an Agilent HP-8453 spectrophotometer with tungsten (VIS) and Deuterium (UV) lamps. The crystal structure of the sample was analyzed using powder X-ray diffraction (XRD) on a PANalytical MPD X'Pert PRO diffractometer. The measurements employed 45 kV, 40 mA Ni-filtered Cu Kα1 radiation at room temperature. X-ray photoelectron spectra (XPS) were obtained on a Thermo-Fisher ESCALAB 250 spectrometer equipped with

a micro-focused, monochromated Al Kα X-ray source operating at 15 kV and a double-focusing, full 180° spherical sector electron analyzer. Scanning electron microscopy (SEM): A Hitachi SU-70 field-SEM with an energy of 5.0 kV was used to take the SEM images. Transmission electron microscopy (TEM): A JEOL JEM1400 TEM was used to obtain the TEM images at 100 kV. Toxic metal concentrations in adsorption and desorption experiments were determined by: Inductively coupled plasma mass spectrometry (ICP-MS): (Agilent 8900 Triple Quadrupole with Electron Multiple Detector) for high sensitivity, detecting metals at parts per billion levels or inductively coupled plasma optical emission spectrometry (ICP-OES) (Charged Coupled Detector) for efficient analysis of higher concentration ranges, detecting metals at parts per million levels.

Adsorption and desorption tests

The adsorption of heavy metal ions from contaminated water was investigated in a series of 20 mL glass vial experiments. Each vial contained 10 mg of adsorbent and 10 mL of toxic metal solution, and the experiments were conducted at room temperature. The extent of metal ion uptake was quantified by ICP-OES or ICP-MS following acidification of the solution with 2% HNO₃. The adsorption capacity (q_e) in mg/g and removal efficiency (% Re) were calculated based on Eqs. 1 and 2, respectively (Bakry et al. 2022; Bakry et al. 2020a, b, c).

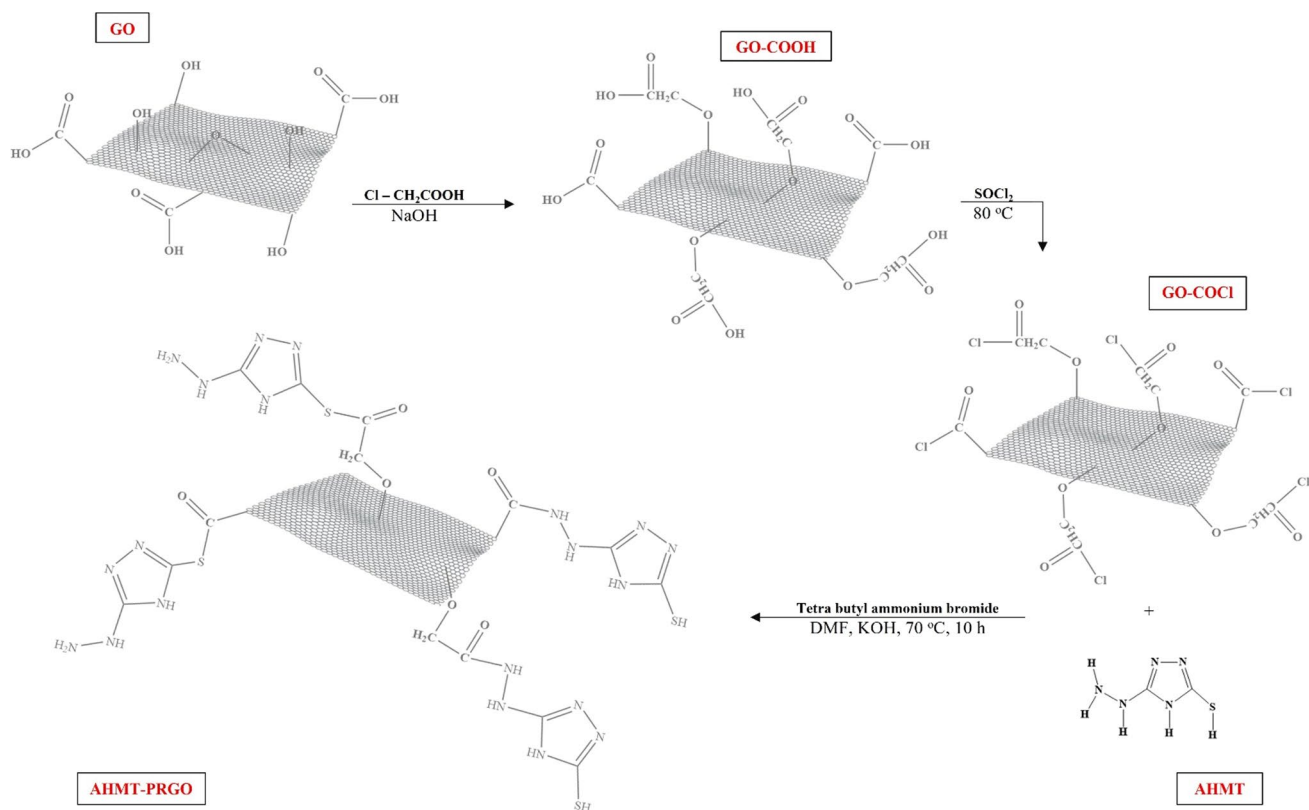
$$q_e = \frac{(C_0 - C_e)V}{m} \quad (1)$$

$$\%R_e = \frac{(C_0 - C_e)}{C_0} \times 100 \quad (2)$$

where C_0 refers to the initial concentration of toxic metal ions present before adsorption in (mg/L), while C_e represents the remaining concentration after reaching equilibrium in (mg/L). The volume of the solution is (V) in (L) and the mass of the adsorbent is (m) in (g).

To recover adsorbed heavy metals, the metal-loaded adsorbents were first collected by centrifugation. After washing with deionized water, they were dried overnight at 60 °C. Then 10 mg of the dried adsorbent was then placed in a 20 mL vial containing a specific concentration of HNO₃ and stirred overnight at room temperature to ensure complete desorption. The concentration of desorbed metal was measured using ICP-OES. Based on these measurements, adsorption capacity (q_d) and desorption efficiency (% De) were calculated using Eqs. 3 and 4, respectively (Bakry et al. 2020a, b, c, 2022).

$$q_d = \frac{C_d V}{m} \quad (3)$$



Scheme 1. The preparation steps of the AHMT-PRGO generation from CMGO and AHMT as starting materials

$$\%D_e = \frac{q_d}{q_e} \times 100 \quad (4)$$

where (C_d) is the concentration of toxic metals in the solution in mg/L after desorption exams, (V) is the volume of the metal ion solutions in (L) after complete desorption tests, and (m) is the mass of heavy metals loaded adsorbents in (g).

Adsorption conditions optimizations and real samples

The adsorption of lead, mercury, and chromium was studied using various experimental parameters at ppm concentration levels. Table S1 details the specific conditions used, including pH range, initial concentrations, contact time, adsorbent dose, and competitive ion presence. The real water samples were collected from various points in Mansoura, Egypt, for heavy metal analysis. The samples were first filtered through a 0.45 mm cellulose membrane to remove impurities. Standard solutions containing different concentrations of heavy metal ions were then added to the samples.

Results and discussion

The AHMT-PRGO design strategy

The AHMT-PRGO adsorbent was synthesized by immobilizing the chelating ligand AHMT onto the surface of graphene oxide (GO) via three main steps as depicted in Scheme 1. In the first step, GO was reacted with sodium hydroxide and chloroacetic acid to form the GO-COOH. This step converted the GO epoxy centers into alcohols via $\text{S}_{\text{N}}1$ ring-opening reactions, followed by the formation of the GO-COOH by reacting chloroacetic acid with GO via a Williamson ether synthesis reaction (Hansen et al. 2020; Ouellette and Rawn 2015). In the second step, the intermediate GO-COCl was prepared through nucleophilic substitution reactions between the GO-COOH and the thionyl chlorides. (F. Awad et al. 2017) In the final step, the chelating ligand AHMT was covalently attached to the GO-COCl surface by the creation of amide bonds via nucleophilic addition/elimination reaction with amines or thiols groups on the AHMT, respectively, using tetrabutylammonium bromide as a catalyst (Awad et al. 2017; Bakry et al. 2020a, b, c). This

synthetic strategy has never been reported in the literature. The AHMT-PRGO adsorbent is novel owing to the characteristic properties of GO, including large surface area and high chemical stability, as well as the presence of nitrogen, oxygen, and sulfur heavy donor atoms with strong chelating characteristics to heavy metals with high selectivity toward mercury.

The AHMT-PRGO characterizations

FTIR spectra

FTIR spectroscopy was employed to confirm the chemical modification of GO by AHMT chelating ligand. The FTIR spectra of AHMT-PRGO, GO-COCl, GO-COOH, and GO are shown in Fig. 1a. The spectra show significant differences due to the appearance of different functional groups on each material. The peak at (3000–3650 cm^{-1}) is common to all four spectra and is attributed to the (O–H) of GO or GO-COOH or the amine (N–H) of AHMT-PRGO stretching vibrations. This peak is absent in the GO-COCl spectrum. The specific region of the spectra from 600 to 2000 cm^{-1} is shown in Fig. 1b. GO and GO-COOH both have peaks at (950, 1045, 1430, 1610, and 1720 cm^{-1}), which are attributed to the (O–H) bending, (C–O) ether or epoxy stretching, (C–O) carboxyl stretching, (C=C) stretching, and (C=O) stretching, vibrations, respectively. GO-COCl has absorption bands at 1680, 1610, 1440, 1330, and 880 cm^{-1} , which are due to the (C=O), (C=C), (C–O) ether, and (C–Cl) stretching vibrations, respectively (Awad et al. 2017; Awad et al.

2018;; Bakry et al. 2020a, b, c). The AHMT-PRGO FTIR spectrum shows peaks at 1698–1618, 1350, and 1200 cm^{-1} , which are assigned to amide (C=O) stretching or (C=C) stretching, (C–O) ether, (C–S), and (C=S) stretching vibrations, respectively (Alzharani et al. 2022; Awad et al. 2018; Awad et al. 2021a, b; Bakry et al. 2020a, b, c). These results confirm the successful modification of GO by AHMT chelating ligands to generate AHMT-PRGO.

XPS analysis

XPS investigation was employed to delve deeper into the surface functional groups of AHMT-PRGO and corroborate FTIR findings. The survey spectrum in Fig. S1 revealed four distinct peaks at 165, 285, 332, and 400 eV, corresponding to C 1s, O 1s, N 1s, and S 2p photoelectrons, respectively (F. Awad et al. 2017; F. S. Awad et al. 2021a, b). A closer look at the C 1s spectrum in Fig. 2a unveiled five peaks at binding energies of 284.1, 284.6, 285.6, 286.2, and 288.3 eV, attributable to (C–C), (C=C), (C–O), (C–OH), and (C–N) photoelectrons (Awad et al. 2017; ; Bakry et al. 2022). This confirms the successful integration of the AHMT chelation ligand onto the GO surface. The XPS spectrum in Fig. 2b revealed two O 1s peaks at 533.6 eV and 532.3 eV, attributable to (C–O) and (O=C) O 1s photoelectrons, respectively (Awad et al. 2017; ; Bakry et al. 2022). This confirms the formation of peptide bonds between the AHMT ligand and the GO surface. Similarly, the N 1s spectrum in Fig. 2c exhibited four peaks at 399.0, 400.0, 400.5, and 401.9 eV, corresponding to (–N=N–), (C–N), (C=N), and (–N=N–)

Fig. 1 FTIR spectra of GO, GO-COOH, GO-COCl, and AHMT-PRGO (a) the entire region (4000–600) cm^{-1} and (b) the definite region (2000–600) cm^{-1}

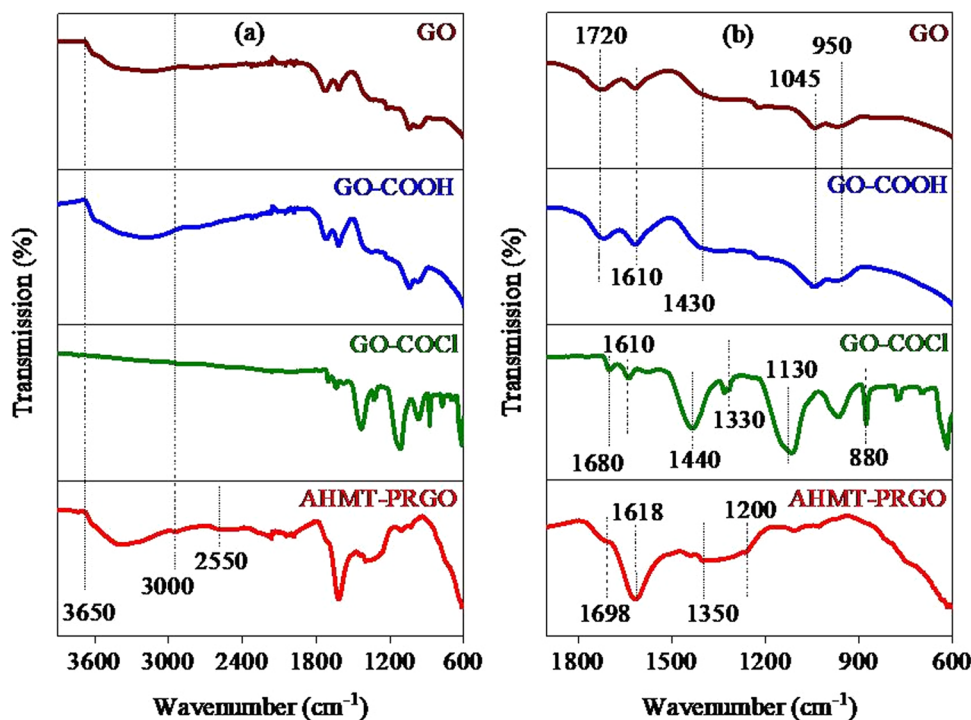
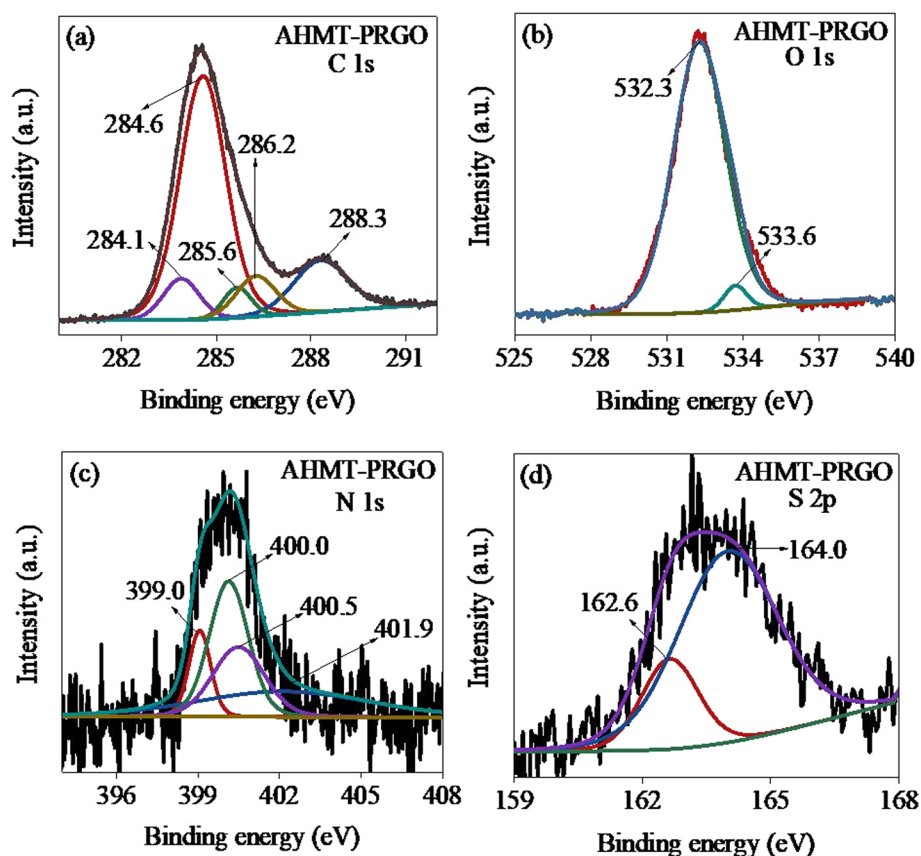


Fig. 2 XPS spectra of AHMT-PRGO, revealing the core-level electronic structure of (a) carbon (C 1s), (b) oxygen (O 1s), (c) nitrogen (N 1s), and (d) sulfur (S 2p) atoms



functional groups, further corroborating the successful ligand incorporation (Bakry et al. 2020a, b, c; Bakry et al. 2020a, b, c). Finally, the S 2p spectrum in Fig. 2d presented peaks at 162.6 eV and 164.0 eV, indicative of ($\text{C}=\text{S}$) and ($\text{S}-\text{C}$) bonds, solidifying the attachment of the AHMT ligand (Bakry et al. 2020a, b, c; Ding et al. 2018). Overall, the XPS analysis aligns with the FTIR findings and conclusively demonstrates the successful functionalization of the GO surface with the AHMT chelation ligand via peptide bond formation.

Raman, UV–VIS, and XRD spectra

The successful modification of GO with the AHMT ligand was confirmed using Raman, UV–VIS, and XRD spectroscopic techniques. Firstly, Raman spectra (Fig. 3a) shows characteristic peaks for all three samples (GO, GO-COOH, and AHMT-PRGO) at 1559 cm^{-1} (G band, sp^2 carbons) and 1347 cm^{-1} (D band, sp^3 carbons and defects). The D/G band intensity ratio increased from 0.92 (GO) to 1.05 (GO-COOH) to 1.07 (AHMT-PRGO), indicating increased disorder due to modification (Awad et al. 2017; ; Bakry et al. 2020a, b, c). Secondly, UV–Vis spectra (Fig. 3b) revealed broad peaks at 230, 249, and 273 nm for GO, GO-COOH, and AHMT-PRGO, respectively, attributed to ($\pi-\pi$) transitions of double bonds. A shoulder peak at 380 nm ($n-\pi^*$)

in GO overlapped with the broad peak in GO-COOH and AHMT-PRGO. Redshifts in the broad peaks and disappearance of the shoulder peak after modification suggest partial GO reduction. Slight discrepancies in the spectra compared to GO and GO-COOH confirms ligand incorporation on the GO surface (Awad et al. 2017; Tran et al. 2023). Finally, XRD patterns (Fig. 3c) show sharp peaks at 11.2° , 10.5° , and 5.6° for GO, GO-COOH, and AHMT-PRGO, respectively (Bakry et al. 2020a, b, c; Bakry et al. 2022; Tran et al. 2023). The peak shift in AHMT-PRGO is attributed to the bulky AHMT ligand increasing the spacing between exfoliated GO layers.

SEM, and TEM images

Figure 4 shows SEM and TEM images of GO and AHMT-PRGO. The AHMT-PRGO adsorbent displays a wrinkled morphology, as observed in the SEM images (Fig. 4b). This wrinkled structure is attributed to the grafting of AHMT ligands onto the PRGO nanosheets, which significantly increases their thickness, as evident in the TEM images (Fig. 4d) (Awad et al. 2017; ; Bakry et al. 2020a, b, c). In summary, the chemical modification of GO with AHMT chelating ligand was successful, as confirmed by various spectroscopic and microscopic techniques. The AHMT ligand was successfully attached to the GO

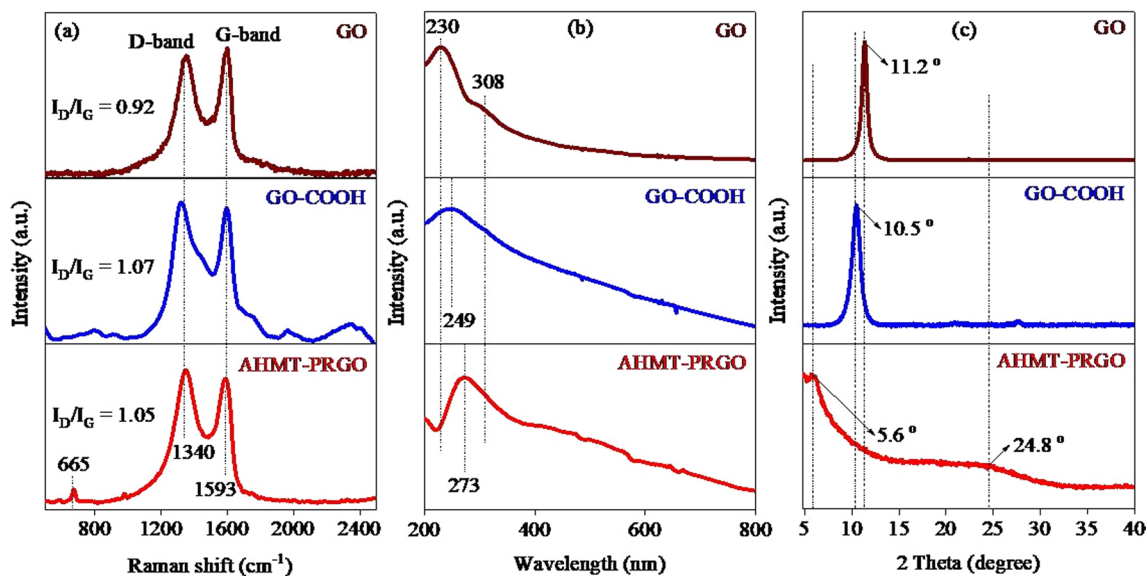
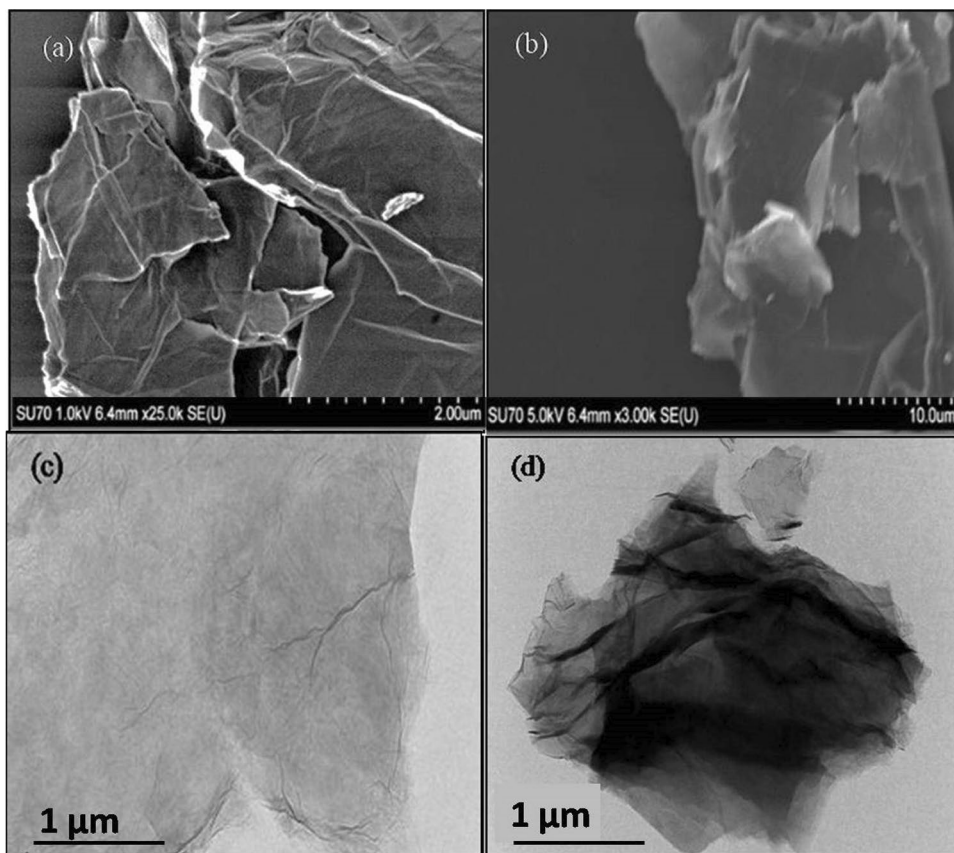


Fig. 3 Spectral characterization of GO, GO-COOH, and AHMT-PRGO nanomaterials: (a) Raman, (b) UV-Vis, and (c) XRD

Fig. 4 SEM and TEM images of GO (a, c) and (b, d) AHMT-PRGO



surface, which changed the structure and properties of GO. The AHMT ligand made the GO more disordered and

reduced, and it also pushed the GO layers further apart. This resulted in a wrinkled-like morphology and a very

thick material that could have potential applications in water treatments.

Heavy metals removal

Influence of solution pH and adsorbent dosage

The acidity (pH) of a solution plays a critical role in how metals bind to an adsorbent surface. As shown in Fig. 5a, for mercury and lead, adsorption capacity significantly increases with increasing pH (from 1 to 6), reaching a maximum of 85.3 mg/g (Hg) and 65.5 mg/g (Pb) at pH 6. This is because higher pH reduces competition from hydrogen ions (H^+), making the adsorbent surface more negatively charged. This negative charge attracts the positively charged mercury and lead ions, similar to opposite ends of a magnet (Awad et al. 2020; Bakry et al. 2020a, b, c). However, chromium (VI) behaves differently. Its adsorption capacity drops from 55.5 to 1.98 mg/g as the pH goes from 1 to 6. This is because under acidic conditions (Fig. S2), chromium (VI) exists as negatively charged chromate ions ($HCrO_4^-$), while the adsorbent's functional groups are positively charged due to protonation. This strong electrostatic attraction between opposite charges leads to optimal removal at low pH (Bakry et al. 2020a, b, c; Din et al. 2023). In essence, pH variation alters the charge of both the adsorbent and the metal ions, impacting their attraction and overall adsorption. The adsorbent's point of zero charge (pHpzc) is where its total surface charge is neutral. For the used adsorbent (AHMT-PRGO), pHpzc is 4.09. Below this pH, the adsorbent is positively charged, repelling positively charged lead and mercury metal ions. As the solution pH increases above pHpzc, the surface becomes negatively charged, attracting Pb^{2+} and mercury Hg^{2+} ions. It's important to note that all experiments were conducted at pH 6 to avoid metal hydroxide ($M(OH)_2$) precipitation at higher pH. However, the exceptional behavior of chromium (VI) is due to its opposite charge at lower pH (El-Wakil et al. 2022). On the other hand, Fig. 5b shows

the effect of adsorbent dosage on the removal of Hg(II), Pb(II), and Cr(VI). The results revealed significant jumps in toxic metals uptakes when the adsorbent dose rises from 5 to 40 g/L due to the enhanced availability of binding sites on the increased adsorbent surface.

Influence of initial concentration and adsorption isotherms

AHMT-PRGO's ability to capture Hg(II), Pb(II), and Cr(VI) was tested by measuring how much it absorbed at different starting concentrations (Fig. 6a). The results revealed that as the initial concentration increased, all three metals were attracted to the AHMT-PRGO's surface more strongly, until it reached its limit. The maximum amounts adsorbed were 370.02 mg/g for Hg(II), 109.56 mg/g for Pb(II), and 165.86 mg/g for Cr(VI). To explain this trend, scientists used a model called the Langmuir adsorption isotherm as the linear form of the Eq. (6) where, C_e is the equilibrium concentration of the adsorbate (mg/L), q_e is the amount adsorbed per unit mass at equilibrium (mg/g), b is the Langmuir constant (L/mg) it is related to the energy of adsorption, and Q_{max} is the Langmuir monolayer adsorption capacity (mg/g) (Bakry et al. 2020a, b, c; Kubra et al. 2023; Murphy et al. 2023).

$$(C_e/q_e = 1/bQ_{max} + C_e/Q_{max}) \quad (5)$$

The data matched this model very closely (Fig. 6b and Table 1), with correlation coefficients (R^2) between 0.988 and 0.999 and R_L values between 0 and 0.1 for all three metals, indicating favorable adsorption. Interestingly, the maximum adsorption capacity (Q_{max}) calculated from the Langmuir model was comparable to the actual amounts measured: 367.83 mg/g for Hg(II), 102.33 mg/g for Pb(II), and 166.08 mg/g for Cr(VI). This suggests that the adsorption process is uniform, with all active sites on the material attracting the metals equally, leading to a single layer

Fig. 5 AHMT-PRGO adsorption capacity for Hg(II), Pb(II), and Cr(VI) Ions. (a) Effect of pH [Conditions: $C_0 = 100$ mg/L for all ions, $T = 298$ K, dose = 0.010 g per 10 mL solution, $t = 420$ min, and pH range = 1–6]. (b) Effect of adsorbent dose [Conditions: $C_0 = 1000$ mg/L for Hg(II) and Pb(II), 100 mg/L for Cr(VI), $T = 298$ K, pH = 6 for Hg(II) and Pb(II), 1 for Cr(VI), $t = 420$ min, dose range = 0.001 to 0.035 g per 10 mL solution]

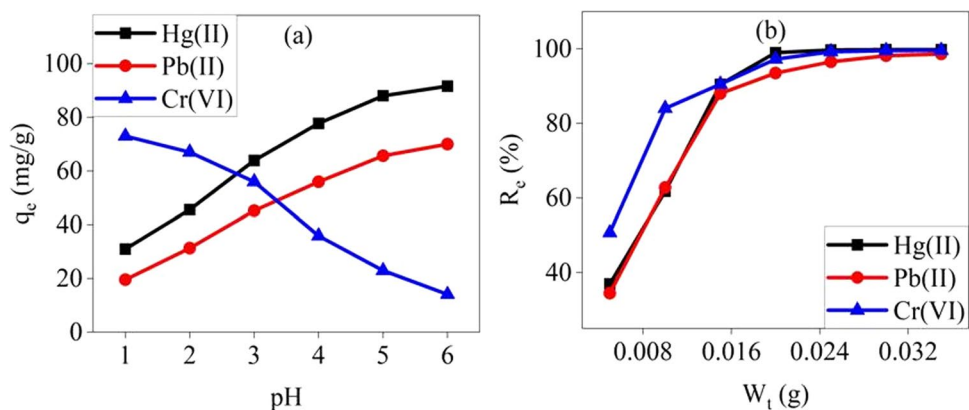


Fig. 6 The efficient adsorption of Hg(II), Pb(II), and Cr(VI) ions onto AHMT-PRGO (a) Initial concentration influence [Conditions: $C_0 = 5\text{--}1000$ mg/L for Hg(II), $25\text{--}500$ mg/L for Pb(II), and $25\text{--}400$ mg/L for Cr(VI), pH = 6 for Hg(II) and Pb(II), 1 for Cr(VI), $T = 298$ K, $t = 420$ min, dose = 0.010 g per 10 mL solution]. (b) Langmuir adsorption isotherm plot. (c) Contact time influence [Conditions: $C_0 = 500$ mg/L for Hg(II), 100 mg/L for Pb(II) and Cr(VI), pH = 6 for Hg(II) and Pb(II), 1 for Cr(VI), $T = 298$ K, $t =$ varies from 5 to 420 min, dose = 0.010 g per 10 mL solution]. (d) The pseudo-second-order kinetic model

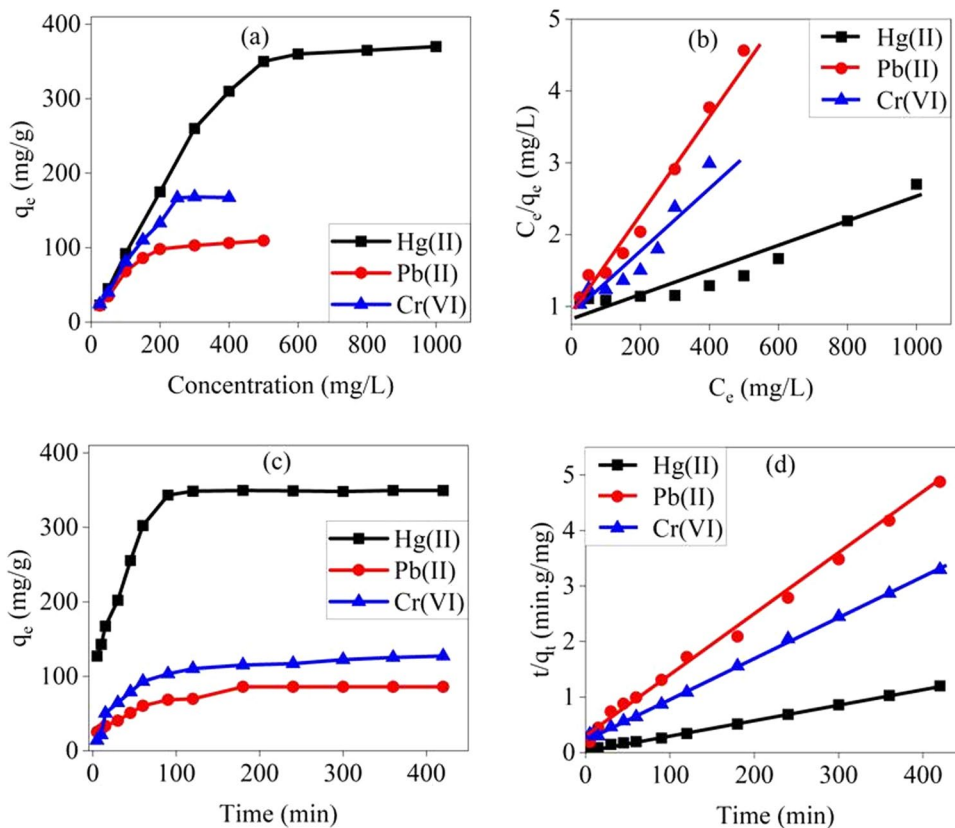


Table 1 Langmuir model analysis of Pb(II), Hg(II), and Cr(VI) adsorption onto AHMT-PRGO

Metal ion	R^2	$Q_{\max, \text{fitted}}$	Q_{exp}	R_L
Hg(II)	0.991	367.83	370.02	0.043
Pb(II)	0.993	102.33	109.56	0.023
Cr(VI)	0.999	166.08	165.86	0.033

covering the surface. The impressive ability of AHMT-PRGO to capture these heavy metals is credited to the sulfur, nitrogen, and oxygen groups present on its high-surface-area graphene oxide (Hasan et al. 2023a, b). These groups act like bonding sites, forming strong connections or electrostatic interactions with the metal ions (Awad et al. 2017, 2020).

The Tempkin isotherm model was used to analyze the heat of adsorption for adsorbate molecules across the surface of nanoparticles (Abdelmonem et al. 2024; Gomaa et al. 2022). This model accounts for variations in adsorption energy with surface coverage. Room temperature experiments were conducted, and the equation used is ($q_e = B \ln(A + C_e)$). Figure S3 presents the results. The Tempkin constant (A), representing the binding affinity (in L/g), and the heat of adsorption (B) in J/mol were determined from the slope and intercept of the linear plot of q_e versus $\ln(C_e)$ (Abdelmonem et al. 2024; H Gomaa et al. 2022). A positive

B values (70.44, 19.72, and 102.02 J/mol for Hg(II), Pb(II), and Cr(VI), respectively) indicates an endothermic adsorption process. The fit to the experimental data was excellent, with an R-squared values of 0.9463, 0.9424, and 0.9565 for Hg(II), Pb(II), and Cr(VI), respectively. Table S2 summarizes these values and the correlation coefficient. Notably, the R-squared value for the Tempkin model is lower than the Langmuir model.

Influence of interaction time and adsorption kinetics

This study investigated how contact time affects the removal of mercury, lead and chromium from water using the AHMT-PRGO. The results, shown in Fig. 6c, indicate that adsorption capacity increases rapidly within the first few hours (5–400 min) and then plateaus as the adsorbent sites become saturated. Equilibrium times for Hg(II), Pb(II), and Cr(VI) were found to be 90, 120, and 180 min, respectively. A mathematical model called the pseudo-second-order kinetic model (SSOKM) was used to analyze the data as the linear form of the equation is ($t/q_t = 1/k_2q_e^2 + t/q_e$); Where: k_2 (g/mole.min) is the second-order rate constant of adsorption, q_e and q_t are the adsorbed amount (mg/g) at equilibrium and at time t (min), respectively (Bobb et al. 2020; Wang and Guo 2020) This model accurately describes the adsorption process, as evidenced by the high correlation coefficients

Table 2 Adsorption rate analysis of Pb(II), Hg(II), and Cr(VI) by AHMT-PRGO using SSOKM

Metal ion	$q_{e, \text{exp}}$ (mg g ⁻¹)	$q_{e, \text{calc}}$ (mg g ⁻¹)	k_2 (g mol ⁻¹ min ⁻¹)	R ²
Hg(II)	349.5	341.3	0.00006	0.994
Pb(II)	167.1	165.8	0.00060	0.995
Cr(VI)	119.2	113.2	0.00138	0.997

(R² > 99%) shown in Fig. 6d. Furthermore, the model's predictions of maximum adsorption capacity (q_t) closely match the experimental values (Table 2). The SSOKM assumes a chemical interaction (chemisorption) between the adsorbent and the heavy metals, involving electron sharing and exchange (Bakry et al. 2020a, b, c; Lam et al. 2023). This is consistent with the presence of nitrogen and oxygen atoms within AHMT-PRGO, which can form strong bonds with the metals. Therefore, AHMT-PRGO is a promising adsorbent for removing Hg(II), Pb(II), and Cr(VI) from water. The adsorption process is rapid and efficient, reaching equilibrium within a few hours. This suggests that chemisorption plays a major role in the removal process.

The equation by Weber and Morries ($q_t = K_{id}t^{0.5} + C$) describes the initial rate of this process, where K_{id} represents the rate constant and C is an intercept value. The intraparticle diffusion model predicts a linear relationship between the amount adsorbed (q_t) and the square root of time ($t^{0.5}$). This linearity indicates that intraparticle diffusion is the dominant mechanism controlling adsorption. The provided data (Fig. S4a and Table S3) seems to support this model at lower concentrations, where the line passes through the origin. Deviations at higher concentrations might be due to changes in mass transfer rates. Furthermore, the Elovich model is used to describe adsorption processes on surfaces that are not uniform (heterogeneous). This equation does not pinpoint a specific mechanism for the interaction between the adsorbate and the adsorbent. The Elovich equation can be expressed in a linear form as ($q_t = 1/\beta \ln \alpha\beta + 1/\beta \ln t$)

where: t: time (minutes), q_t : amount of adsorbate adsorbed at time t (mg/g), α : initial adsorption rate (mg/g min), β : constant related to surface coverage and activation energy (g/mg). The constants α and β can be determined by fitting the linear equation to experimental data (see Table S4 and Fig. S4b). A good linear fit with an R-squared value greater than 0.95 at lower concentrations suggests that diffusion is the rate-limiting step in the adsorption process. However, the initial adsorption rate (α) does not show a consistent trend with increasing metal ions concentration.

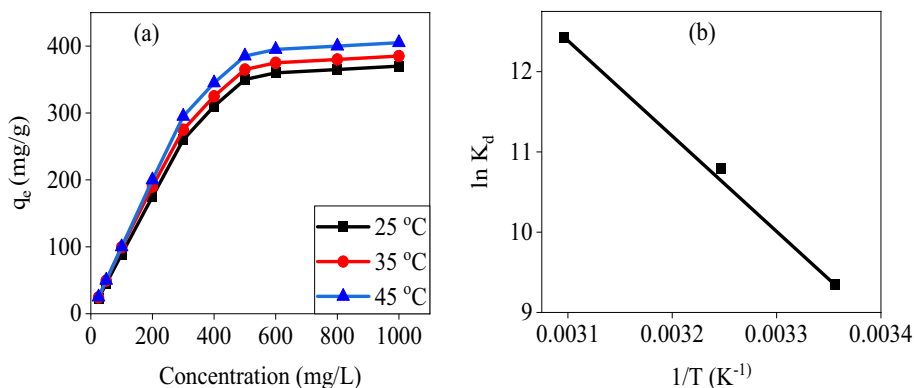
Adsorption thermodynamics

This study investigated the influence of temperature on the adsorption capacity of Hg(II) ions using AHMT-PRGO. The experiments were conducted under constant conditions: pH 6, contact time 420 min, and AHMT-PRGO dosage of 5 mg/L. The Hg(II) solution concentrations ranged from 5 to 1000 mg/L. Three temperatures were tested: 25, 35 °C. The results in Fig. 7a revealed that the maximum adsorption capacity for Hg(II) increased from 370 to 405 mg/g as the temperature rose from 25 to 45 °C. This can be attributed to the higher mobility and kinetic energy of ions in solution at elevated temperatures. Equations 7 and 8 were used to calculate the thermodynamic functions (ΔG° , ΔH° , and ΔS°) of the adsorption process (Hassanien Gomaa et al. 2023a, b). Here, ΔG° represents the change in free energy, ΔH° represents the change in enthalpy, ΔS° represents the change in entropy, R is the gas constant, T is the temperature, and Kc is the equilibrium constant. The data and the calculated

Table 3 Thermodynamic parameters for the adsorption of Hg(II) on AHMT-PRGO

Metal ion	T (K)	ΔG (kJ/mol)	ΔH (kJ/mol)	ΔS (kJ/mol)	R ²
Hg(II)	298	-15.79	108.44	0.439	0.9851
	308	-16.48			
	323	-17.51			

Fig. 7 (a) Effect of temperature on the removal of Hg(II) using AHMT-PRGO [conditions; C₀ = 25–1000 mg/L Hg(II), 5–1000 mg/L, pH = 6, T = 25, 35, and 45 °C, t = 6 h, dose = 5 mg/5 mL]. (b) Plots of ln(K_d) vs T⁻¹ for the estimation of the thermodynamics parameters of the adsorption process for Hg



thermodynamic parameters are presented in Fig. 7b and Table 3, respectively.

$$\Delta G^\circ = -RT \ln K_c \quad (6)$$

$$\ln K_c = \left(\frac{\Delta S^\circ}{R} \right) - \left(\frac{\Delta H^\circ}{R} \right) \frac{1}{T} \quad (7)$$

The negative ΔG° values for adsorbent indicate that the adsorption process is spontaneous. The positive ΔH° value confirms the endothermic nature of adsorption, which aligns with the observed increase in adsorption capacity at higher temperatures (Hassanien et al. 2023a). The positive ΔS° values suggest an increase in disorder at the solid-solution interface during adsorption (Hassanien et al. 2023b). This is likely due to the release of water solvent molecules from the metal ions back into the solution.

Selectivity of AHMT-PRGO for Hg(II) and reusability

AHMT-PRGO was shown to selectively adsorb Hg(II) out of a mixture of other metal ions, including Pb(II), Cu(II), Co(II), Cr(IV), As(IV), Cd(II), Ni(II), and Zn(II) (Fig. 8a). This preference for Hg(II) is due to two main factors. First, Hg(II) is classified as a soft acid, and the sulfur functional groups on the AHMT-PRGO surface are considered soft bases. This creates a strong attraction between Hg(II) and AHMT-PRGO, leading to the formation of stable Hg(II) complexes. Second, the size and shape of the metal ions also play a role. Hg(II) has a larger ionic radius than Cd(II), for instance. Some materials have pores or binding sites that are specifically sized to allow Hg(II) to enter and bind

effectively, while excluding smaller ions like Cd(II) (Abebe and Murthy 2022; Awad et al. 2021a, b; Hassanien et al. 2023). These properties make AHMT-PRGO a promising material for Hg(II) removal from wastewater and other contaminated solutions containing multiple heavy metals. Furthermore, studies employing nitric acid to regenerate the AHMT-PRGO adsorbent demonstrate its exceptional desorption capacity for heavy metals. As shown in Table S5, desorption efficiencies for Hg(II) and Pb(II) increase from 80.30 and 85.60%, respectively, to 99.34% and 99.78% with increasing acid concentration (0.5–1.5 M). This efficient and cost-effective regeneration process, illustrated in Fig. 8b for Hg(II) ions, coupled with minimal adsorption decline over four cycles (reloading efficiency > 92%), positions AHMT-PRGO as a promising candidate for heavy metal removal from industrial wastewater.

Real samples

To assess the practicality and efficiency of the AHMT-PRGO as an adsorbent, its ability to detect trace levels of Hg(II) in various water samples was investigated. Water samples were collected from different locations in Mansoura, Egypt, and filtered using a 0.45 mm cellulose membrane to remove solid contaminants. Standard Hg(II) solutions were then spiked into the filtered water samples. The results (Table 4) obtained indicated that AHMT-PRGO successfully recovered Hg(II) with recoveries ranging from 94.0 to 100% and relative standard deviation (RSD) values below 5%. These findings demonstrate the feasibility of utilizing AHMT-PRGO for determining Hg(II) concentrations in various water sample.

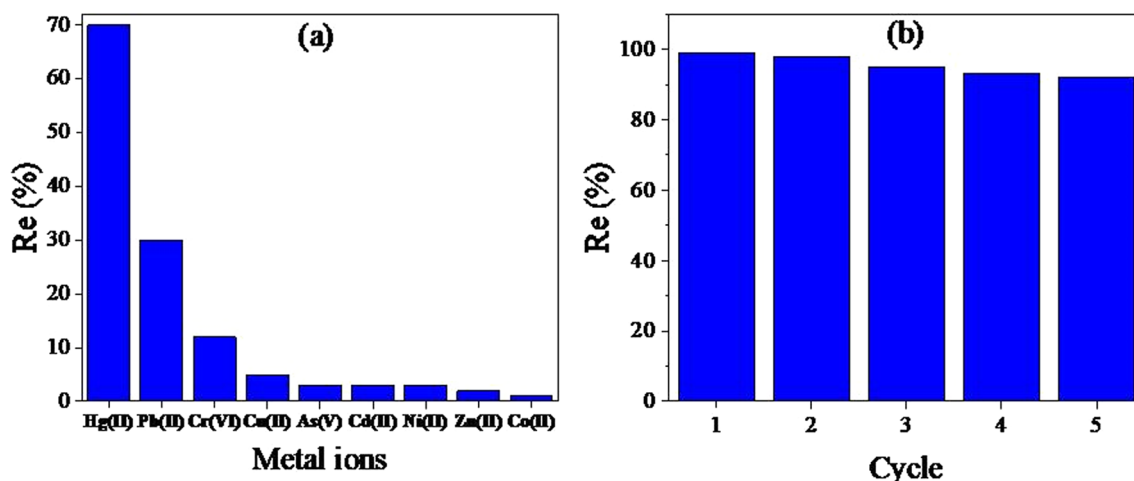


Fig. 8 (a) Removal of nine mixed metal ions from a solution using AHMT-PRGO [Conditions $C_0=250$ mg/L, pH=6, adsorbent dose 1 g/L, $T=298$ K, and $t=420$ min]. (b) Recycling of the AHMT-PRGO for Hg(II) ions

Table 4 Comparing Hg(II) levels in different water sources: tap water, Nile River and groundwater

Samples	Added amount of mercury ions ($\mu\text{g L}^{-1}$)	Found the amount of mercury ions ($\mu\text{g L}^{-1}$)	%Recovery
Tap water	–	0.190	–
	2.0	2.185	99.75
	4.0	4.182	99.80
	8.0	8.190	100.0
River water	–	0.410	–
	2.0	2.362	97.60
	4.0	4.334	98.10
	8.0	8.332	99.02
Ground water	–	0.32	–
	2.0	2.25	96.50
	4.0	4.17	96.25
	8.0	8.19	98.37
Waste water	–	6.3	–
	2.0	8.18	94.0
	4.0	10.1	95.0
	8.0	13.93	95.37

Proposed adsorption and desorption mechanism

The proposed mechanisms for the adsorption of mercury ions on the surface of the adsorbent are depicted in Scheme 2. According to the structure of adsorbent-Hg,

uptake of mercury takes place by chemisorption through forming coordination bonds between mercury ions in the solution and the functional groups on the surface of the adsorbent. According to the structure of the adsorbent, there are nitrogen, oxygen, and sulfur heavy donor atoms which act as Lewis's bases while heavy metals can act as Lewis's acids (Hasan et al. 2023a, b). Therefore, Lewis bases donate their lone pairs of electrons to Lewis's acids which have empty orbitals and form stable metal complexes (Awual et al. 2016). However, to desorb mercury ions from the solution nitric acid was used to release a large amount of proton in the solution. Therefore, protons can release mercury ions from the adsorbent because those protons have higher coordination ability than lead ions (Awad et al. 2021a, b; Bakry et al. 2020a, b, c; Yuan et al. 2021).

Mercury's presence on the surface of AHMT-PRGO was confirmed using XPS analysis. The high-resolution Hg 4f spectrum (Fig. 9a) showed two peaks at 102 and 106 eV, corresponding to Hg 4f^{7/2} and Hg 4f^{5/2}, respectively (Bakry et al. 2020a, b, c). These peaks were shifted to higher binding energies compared to free mercury atoms, indicating strong interactions between mercury ions and AHMT-PRGO's functional groups, likely forming mercury complexes. Further evidence for this interaction came from the O 1s spectrum (Fig. 9b). After mercury adsorption, it deconvoluted into four peaks at 529.8, 531.0, 531.6, and 533.3 eV. Notably, the peaks at 531.6 and 533.3 eV were significantly shifted to lower binding energies compared to

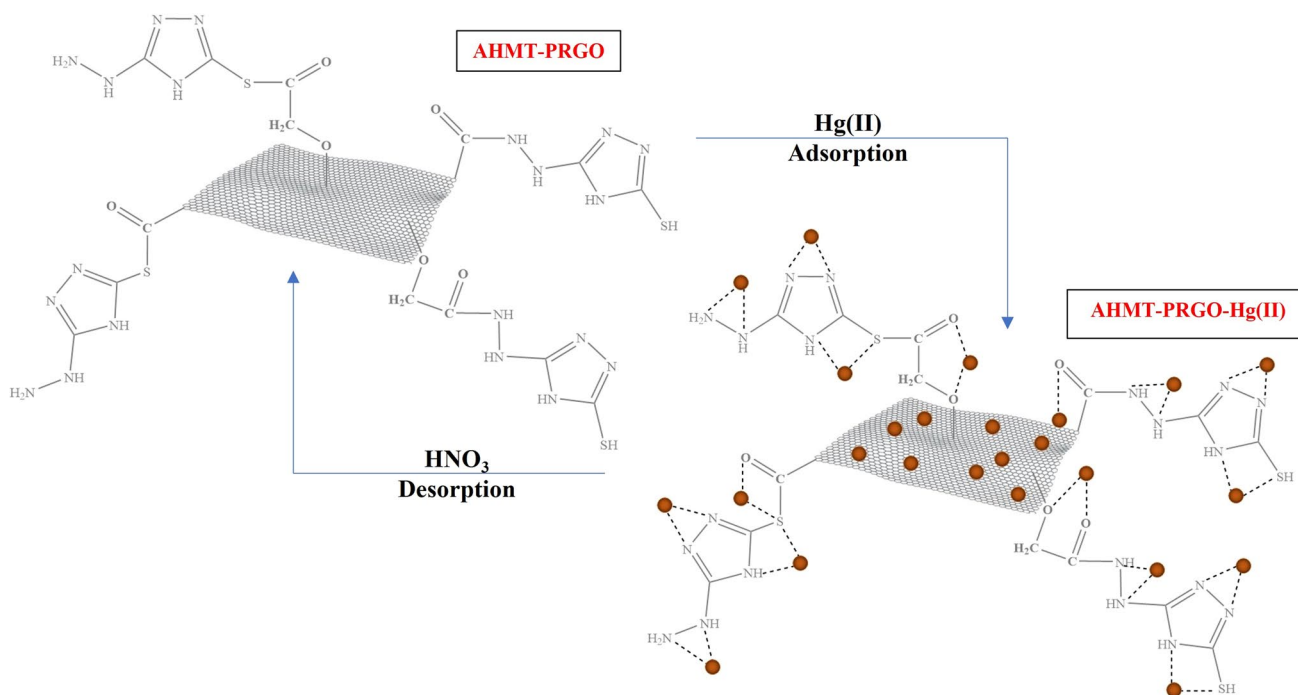
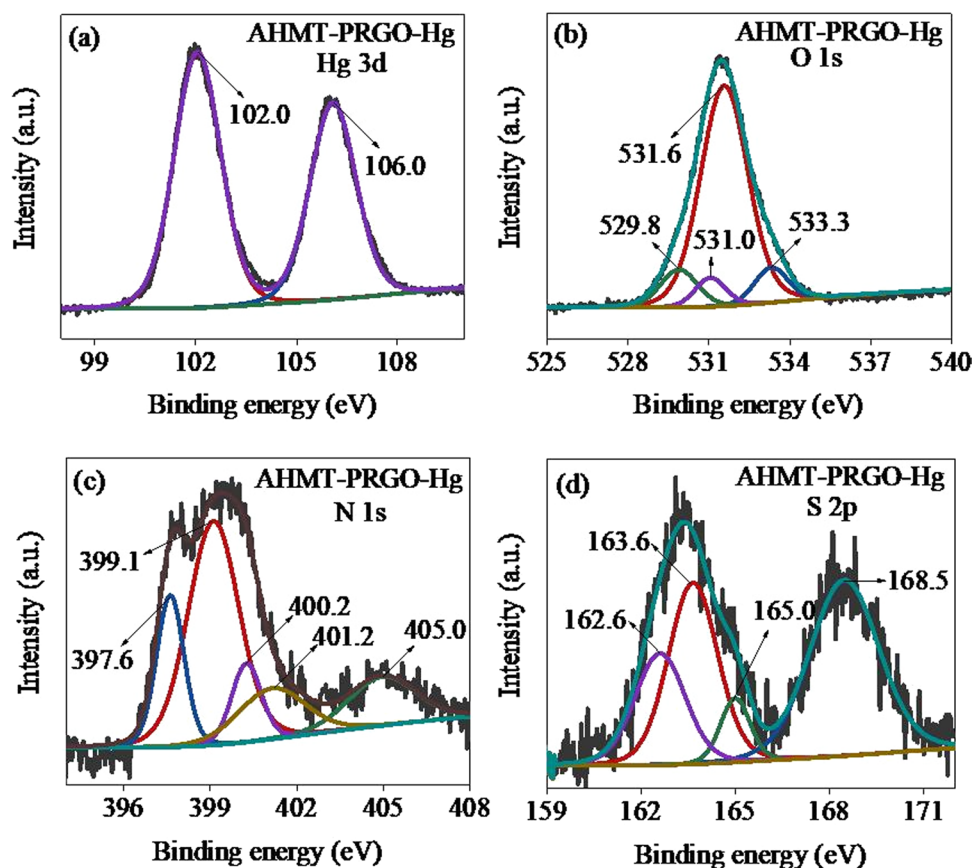
**Scheme 2.** Proposed Hg(II) removal pathways on AHMT-PRGO adsorbent

Fig. 9 XPS of AHMT-PRGO after Hg adsorption (a) Hg 4f, (b) O 1s, (c) N 1s, and (d) S 2p



the original spectrum. This, along with the presence of peaks at 529.8 and 531.0 eV, suggests the formation of oxygen-mercury bonds (Awad et al. 2017;; Bakry et al. 2020a, b, c). Similarly, the N 1s spectrum after mercury adsorption (Fig. 9c) revealed five peaks at 397.6, 399.1, 400.2, 401.2, and 405.0 eV. The first four peaks were shifted to lower binding energies compared to the original N 1s spectrum (Bakry et al. 2020a, b, c; Bakry et al. 2020a, b, c). Additionally, the presence of a peak at 405 eV provides further evidence for mercury ion coordination with AHMT-PRGO's nitrogen functional groups. Finally, the S 2p spectrum after mercury adsorption (Fig. 9d) showed four peaks at 162.6, 163.6, 165.0, and 168.5 eV. These peaks also differed from the original S 2p spectrum, suggesting the involvement of sulfur atoms in coordinating mercury ions (Awad et al. 2017, 2018) Therefore, the XPS analysis strongly suggests that chelation by AHMT-PRGO's oxygen, nitrogen, and sulfur functional groups is the primary mechanism for mercury adsorption on its surface.

Comparing the AHMT-PRGO with other adsorbents

The exceptional adsorption capacity of AHMT-PRGO for mercury was definitively demonstrated by surpassing the performance of all previously reported adsorbents listed in

Table 5. Its remarkable uptake of 370 mg/g for Hg(II), the highest value shown, stands as a testament to its superiority. This exceptional performance can be attributed to the combination of its high surface area, strong chemical stability, and the presence of nitrogen, oxygen, and sulfur—heavy donor atoms known for their strong chelating ability towards heavy metals, particularly mercury.

Conclusions and outlooks

This study successfully synthesized a novel adsorbent, AHMT-PRGO, for removing harmful heavy metals like mercury, lead, and chromium from water. The AHMT-PRGO was designed by covalently attaching a powerful chelating agent, 4-amino-3-hydrazino-5-mercapto-1,2,4-triazole (AHMT), to the surface of specially treated graphene oxide (CMGO) through a three-step process. Various characterization techniques confirmed the successful incorporation of the AHMT ligand onto the GO surface like UV–Vis, FTIR, Raman, XRD, XPS, SEM, and TEM confirm the successful modification. The AHMT-PRGO demonstrated excellent adsorption capacity for Hg(II), Pb(II), and Cr(VI) with maximum values of 370.0, 136.2, and 109.6 mg/g, respectively, which is superior to most previously reported adsorbents.

Table 5 The AHMT-PRGO new adsorbent vs. established materials: mercury removal performance

Adsorbent	q_e (mg/g)	Time (min)	Ref
Partially reduced GO	110.2	20	Tene et al. (2022)
Thiol-functionalized MOF	171.5	–	Ding et al. (2018)
Thiol-functionalized GO	49.6	2160	Sun et al. (2023a, b)
Aminothiazole modified activated carbon	252.5	60	Waly et al. (2021)
Thiosemicarbazide-grafted GO	231.0	30	Sitko et al. 2021)
ND-CPC	257.0	200	Bakry et al. (2020a; b, c)
polyamine modified RGO	63.8	45	Yap et al. (2020)
Thiol-modified GO/Fe–Mn composite	112.03		Huang et al. (2020)
Glutathione-functionalized NiFe ₂ O ₄ /GO	272.94		Khorshidi et al. (2020)
Magnetic graphene oxide-chitosan nanohybrid	339.82	8	Bulin et al. (2023)
Fe–Mn oxide modified biochar	86.82		Sun et al. (2023a, b)
Triazine-Based Functionalized AC	292.6		El-Wakil et al. (2022)
sulfur-coated magnetic MWCNT	62.11		Fayazi (2020)
AHMT-PRGO	370.0	60	Current work

Moreover, the equilibrium contact times are impressively fast, reaching 60, 30, and 400 min for Hg(II), Pb(II), and Cr(VI), respectively. Additionally, the AHMT-PRGO exhibited high selectivity for Hg(II) ions in a mixture of nine heavy metal ions and showed good reusability after multiple adsorption–desorption cycles. Furthermore, AHMT-PRGO effectively removed heavy metal ions from real water samples. The novelty of AHMT-PRGO lies in the combination of a multidentate ligand for strong and selective binding with the high surface area and stability offered by covalently bonded graphene oxide. This combination offers advantages over traditional adsorbents in terms of adsorption capacity, selectivity, and reusability. AHMT-PRGO has great potential for application in water treatment technologies for removing toxic heavy metals from wastewater.

Supporting Information

The experimental setup for lead (II), mercury(II), and chromium(VI) adsorption using AHTM-PRGO (Table S1). Evaluating the regeneration of AHTM-PRGO for Hg(II) and Pb(II) removal using diverse eluents after initial adsorption at 1000 ppm (Table S2). Survey spectrum of XPS of AHMT-PRGO (Fig. S1).

Supplementary Information The online version contains supplementary material available at <https://doi.org/10.1007/s13201-024-02234-y>.

Acknowledgement The authors gratefully acknowledge the funding of the Deanship of Graduate Studies and Scientific Research, Jazan University, Saudi Arabia, through project number: (RG24-S015).

Funding Not applicable.

Data availability The datasets used and/or analyzed during the current study are available from the corresponding author on reasonable request.

Declarations

Conflict of interest There are no conflict to declare.

Ethical Standards For this type of study formal consent is not required.

Open Access This article is licensed under a Creative Commons Attribution 4.0 International License, which permits use, sharing, adaptation, distribution and reproduction in any medium or format, as long as you give appropriate credit to the original author(s) and the source, provide a link to the Creative Commons licence, and indicate if changes were made. The images or other third party material in this article are included in the article's Creative Commons licence, unless indicated otherwise in a credit line to the material. If material is not included in the article's Creative Commons licence and your intended use is not permitted by statutory regulation or exceeds the permitted use, you will need to obtain permission directly from the copyright holder. To view a copy of this licence, visit <http://creativecommons.org/licenses/by/4.0/>.

References

- Abdelmonem HA, Hassanein TF, Sharafeldin HE, Gomaa H, Ahmed AS, Abdel-lateef AM (2024) Cellulose-embedded polyacrylonitrile/amidoxime for the removal of cadmium (II) from wastewater: adsorption performance and proposed mechanism. *Colloids Surf A* 684:133081
- Abebe B, Murthy HCA (2022) Insights into ZnO-based doped porous nanocrystal frameworks. *RSC Adv* 12:5816–5833. <https://doi.org/10.1039/d1ra09152b>
- Adel M, Ahmed MA, Elabiad MA, Mohamed AA (2022) Removal of heavy metals and dyes from wastewater using graphene oxide-based nanomaterials: a critical review. *Environ Nanotechnol Monitor Manag* 18:100719. <https://doi.org/10.1016/j.enmm.2022.100719>
- Al-wakeel K, Ahmed M, Akhdhar A, Sulaiman M, Khan Z (2022) Recent advances in alginate-based adsorbents for heavy metal

- retention from water: a review. *Desalin Water Treat* 272:50–74. <https://doi.org/10.5004/dwt.2022.28834>
- Ali Q, Zia MA, Kamran M, Shabaan M, Zulfiqar U, Ahmad M (2023) Nanoremediation for heavy metal contamination: a review. *Hybrid Adv* 4:100091. <https://doi.org/10.1016/j.hybadv.2023.100091>
- Alzharani A, Shehab MK, Rodene DD, Ahmed JU, Bakry AM, Kaid MM (2022) Surface modification of partially reduced graphene oxide for advanced electrode material in rechargeable sodium batteries. *Energy Fuels* 36(9):4967–4977. <https://doi.org/10.1021/acs.energyfuels.2c00193>
- Asghar F, Shakoor B, Fatima S, Munir S, Razzaq H, Naheed S (2022) Fabrication and prospective applications of graphene oxide-modified nanocomposites for wastewater remediation. *RSC Adv* 12(19):11750–11768. <https://doi.org/10.1039/D2RA00271J>
- Awad F, Abouzeid K, El-Maaty W, El-Wakil A, El-Shall MS (2017) Efficient removal of heavy metals from polluted water with high selectivity for Mercury(II) by 2-Imino-4-Thiobiuret partially reduced graphene oxide (IT-PRGO). *ACS Appl Mater Interfaces*. <https://doi.org/10.1021/acsami.7b10021>
- Awad F, Abouzeid K, El-Maaty W, El-Wakil A, El-Shall MS (2018) Effective removal of mercury(II) from aqueous solutions by chemically modified graphene oxide nanosheets. *Arab J Chem*. <https://doi.org/10.1016/j.arabjc.2018.06.018>
- Awad FS, AbouZied KM, Abou El-Maaty WM, El-Wakil AM, Samy El-Shall M (2020) Effective removal of mercury(II) from aqueous solutions by chemically modified graphene oxide nanosheets. *Arab J Chem* 13(1):2659–2670. <https://doi.org/10.1016/j.arabjc.2018.06.018>
- Awad FS, AbouZied KM, Bakry AM, Abou El-Maaty WM, El-Wakil AM, El-Shall MS (2021a) Polyacrylonitrile modified partially reduced graphene oxide composites for the extraction of Hg(II) ions from polluted water. *J Mater Sci* 56(13):7982–7999. <https://doi.org/10.1007/s10853-021-05797-2>
- Awad FS, Bakry AM, Ibrahim AA, Lin A, El-Shall MS (2021b) Thiol- and amine-incorporated UIO-66-NH₂ as an efficient adsorbent for the removal of mercury(II) and phosphate ions from aqueous solutions. *Ind Eng Chem Res* 60(34):12675–12688. <https://doi.org/10.1021/acs.iecr.1c01892>
- Awual ME, Salman MS, Hasan MM, Hasan MN, Kubra KT, Sheikh MC (2024) Ligand imprinted composite adsorbent for effective Ni (II) ion monitoring and removal from contaminated water. *J Ind Eng Chem* 131:585–592
- Awual MR (2017) Novel nanocomposite materials for efficient and selective mercury ions capturing from wastewater. *Chem Eng J* 307:456–465
- Awual MR (2019) Innovative composite material for efficient and highly selective Pb (II) ion capturing from wastewater. *J Mol Liq* 284:502–510
- Awual MR, Alharthi NH, Okamoto Y, Karim MR, Halim ME, Hasan MM (2017) Ligand field effect for Dysprosium (III) and Lutetium (III) adsorption and EXAFS coordination with novel composite nanomaterials. *Chem Eng J* 320:427–435
- Awual MR, Hasan MM, Eldesoky GE, Khaleque MA, Rahman MM, Naushad M (2016) Facile mercury detection and removal from aqueous media involving ligand impregnated conjugate nanomaterials. *Chem Eng J* 290:243–251
- Awual MR, Hasan MN, Hasan MM, Salman MS, Sheikh MC, Kubra KT (2023) Green and robust adsorption and recovery of Europium (III) with a mechanism using hybrid donor conjugate materials. *Sep Purif Technol* 319:124088
- Bakry A, Awad F, Bobb J, Ibrahim A, El-Shall MS (2020a) Melamine-based functionalized graphene oxide and zirconium phosphate for high performance removal of mercury and lead ions from water. *RSC Adv* 10:37883–37897
- Bakry AM, Alamier WM, Salama RS, Samy El-Shall M, Awad FS (2022) Remediation of water containing phosphate using ceria nanoparticles decorated partially reduced graphene oxide (CeO₂-PRGO) composite. *Surfaces Interfaces* 31:102006. <https://doi.org/10.1016/j.surfin.2022.102006>
- Bakry AM, Awad FS, Bobb JA, El-Shall MS (2020b) Multifunctional binding sites on nitrogen-doped carboxylated porous carbon for highly efficient adsorption of Pb (II), Hg (II), and Cr (VI) ions. *ACS Omega* 5(51):33090–33100
- Bakry AM, Awad FS, Bobb JA, El-Shall MS (2020c) Multifunctional binding sites on nitrogen-doped carboxylated porous carbon for highly efficient adsorption of Pb(II), Hg(II), and Cr(VI) ions. *ACS Omega* 5(51):33090–33100. <https://doi.org/10.1021/acscomega.0c04695>
- Bobb JA, Awad FS, Moussa S, El-Shall MS (2020) Laser synthesis of magnetite-partially reduced graphene oxide nanocomposites for arsenate removal from water. *J Mater Sci* 55(13):5351–5363. <https://doi.org/10.1007/s10853-020-04363-6>
- Bulin C, Zheng R, Song J, Bao J, Xin G, Zhang B (2023) Magnetic graphene oxide-chitosan nanohybrid for efficient removal of aqueous Hg (II) and the interaction mechanism. *J Mol Liq* 370:121050
- da Silva VD, Zaleska K, Petrovski Z, Buarque CD, Branco LC, Esteves PM (2023) Covalent organic frameworks as promising materials for the removal of metal and organic pollutants from water. *Mater Today Sustain* 21:100279. <https://doi.org/10.1016/j.mtsust.2022.100279>
- Din I, Khan I, Aziz F, Sher A, Hakim S (2023) Graphene oxide nanoparticles a remedy for chromium pollution. *Curr Res Green Sustain Chem* 7:100372. <https://doi.org/10.1016/j.crgsc.2023.100372>
- Ding L, Luo X, Shao P, Yang J, Sun D (2018) Thiol-functionalized Zr-based metal-organic framework for capture of Hg(II) through a proton exchange reaction. *ACS Sustain Chem Eng* 6(7):8494–8502. <https://doi.org/10.1021/acssuschemeng.8b00768>
- El-Wakil AM, Waly SM, Abou El-Maaty WM, Waly MM, Yilmaz M, Awad FS (2022) Triazine-based functionalized activated carbon prepared from water hyacinth for the removal of Hg²⁺, Pb²⁺, and Cd²⁺ ions from water. *ACS Omega* 7(7):6058–6069
- Fayazi M (2020) Removal of mercury (II) from wastewater using a new and effective composite: sulfur-coated magnetic carbon nanotubes. *Environ Sci Pollut Res* 27(11):12270–12279
- Feng T, Xu J, Yu C, Cheng K, Wu Y, Wang Y (2019) Graphene oxide wrapped melamine sponge as an efficient and recoverable adsorbent for Pb(II) removal from fly ash leachate. *J Hazard Mater* 367:26–34. <https://doi.org/10.1016/j.jhazmat.2018.12.053>
- Gendy EA, Ifthikar J, Ali J, Oyekunle DT, Elkhlfia Z, Shahib II (2021) Removal of heavy metals by covalent organic frameworks (COFs): a review on its mechanism and adsorption properties. *J Environ Chem Eng* 9(4):105687. <https://doi.org/10.1016/j.jece.2021.105687>
- Gomaa H, Emran MY, Elsenety MM, Abdel-Rahim RD, Deng Q, Gadallah MI (2023a) Selective removal of thorium ions from aqueous solutions using a hybrid mesoporous adsorbent as benzenesulfonamide-derivative@ ZrO₂. *J Water Process Eng* 51:103436
- Gomaa H, Emran MY, Elsenety MM, Abdel-Rahim RD, Deng Q, Gadallah MI (2023b) Detection and selective removal strategy of thorium ions using a novel fluorescent ligand and hybrid mesoporous γ -Al₂O₃-like nanoneedles. *ACS Sustain Chem Eng* 11(6):2127–2138
- Gomaa H, Sayed A, Mahross M, Abdel-Hakim M, Othman IM, Li J (2022) A hybrid spongy-like porous carbon-based on azopyrazole-benzenesulfonamide derivative for highly selective Fe³⁺-adsorption from real water samples. *Microporous Mesoporous Mater* 330:111578
- Gomaa H, Shenashen MA, Cheira MF, Sueki K, El-Nasr TAS, Selim MM (2023c) Green extraction of uranium (238U) from natural radioactive resources. *Chem Eng J* 461:142014
- Gomaa H, Shenashen MA, Cheira MF, Sueki K, El-Nasr TAS, Selim MM (2023d) A novel, spongy mesoporous hybrid bio-adsorbents

- derived from agricultural waste for highly selective thorium recovery. *J Clean Prod* 402:136819
- Groz dov D, Zinicovscaia I (2023) Mesoporous materials for metal-laden wastewater treatment. *Materials* (basel). <https://doi.org/10.3390/ma16175864>
- Hansen T, Vermeeren P, Haim A, Dorp M, Codée J, Bickelhaupt FM (2020) Regioselectivity of epoxide ring-openings via SN2 reactions under basic and acidic conditions. *Eur J Org Chem* 2020:3822–3828. <https://doi.org/10.1002/ejoc.202000590>
- Hasan MM, Kubra KT, Hasan MN, Awual ME, Salman MS, Sheikh MC (2023a) Sustainable ligand-modified based composite material for the selective and effective cadmium (II) capturing from wastewater. *J Mol Liq* 371:121125
- Hasan MN, Salman MS, Hasan MM, Kubra KT, Sheikh MC, Rehan AI (2023b) Assessing sustainable Lutetium (III) ions adsorption and recovery using novel composite hybrid nanomaterials. *J Mol Struct* 1276:134795
- Huang R, Lv J, Chen J, Zhu Y, Zhu J, Wågberg T (2023) Three-dimensional porous high boron-nitrogen-doped carbon for the ultrasensitive electrochemical detection of trace heavy metals in food samples. *J Hazard Mater* 442:130020. <https://doi.org/10.1016/j.jhazmat.2022.130020>
- Huang Y, Wang M, Gong Y, Zeng EY (2020) Efficient removal of mercury from simulated groundwater using thiol-modified graphene oxide/Fe–Mn composite in fixed-bed columns: experimental performance and mathematical modeling. *Sci Total Environ* 714:136636
- Khazaei M, Nasser S, Ganjali MR, Khoobi M, Nabizadeh R, Gholibegloo E (2018) Selective removal of lead ions from aqueous solutions using 1,8-dihydroxyanthraquinone (DHAQ) functionalized graphene oxide; isotherm, kinetic and thermodynamic studies. *RSC Adv* 8(11):5685–5694. <https://doi.org/10.1039/C7RA13603J>
- Khorshidi P, Shirazi RHSM, Miralinaghi M, Moniri E, Saadi S (2020) Adsorptive removal of mercury (II), copper (II), and lead (II) ions from aqueous solutions using glutathione-functionalized NiFe₂O₄/graphene oxide composite. *Res Chem Intermed* 46:3607–3627
- Kubra KT, Hasan MM, Hasan MN, Salman MS, Khaleque MA, Sheikh MC (2023) The heavy lanthanide of Thulium (III) separation and recovery using specific ligand-based facial composite adsorbent. *Colloids Surf A* 667:131415
- Lam ITY, Choi S-J, Lu D, Kim Y (2023) Functionalized metal–organic frameworks for heavy metal ion removal from water. *Nanoscale* 15(24):10189–10205. <https://doi.org/10.1039/D3NR02250A>
- Murphy OP, Vashishtha M, Palanisamy P, Kumar KV (2023) A review on the adsorption isotherms and design calculations for the optimization of adsorbent mass and contact time. *ACS Omega* 8(20):17407–17430. <https://doi.org/10.1021/acsomega.2c08155>
- Ouellette RJ, Rawn JD (2015) 16—ethers and epoxides. In: Ouellette RJ, Rawn JD (eds) *Organic chemistry study guide*. Elsevier, Boston, pp 277–297
- Rehan AI, Rasee AI, Awual ME, Waliullah R, Hossain MS, Kubra KT (2023) Improving toxic dye removal and remediation using novel nanocomposite fibrous adsorbent. *Colloids Surf A* 673:131859
- Richardson SD, Ternes TA (2022) Water analysis: emerging contaminants and current issues. *Anal Chem* 94(1):382–416. <https://doi.org/10.1021/acs.analchem.1c04640>
- Salman MS, Hasan MN, Hasan MM, Kubra KT, Sheikh MC, Rehan AI (2023) Improving copper (II) ion detection and adsorption from wastewater by the ligand-functionalized composite adsorbent. *J Mol Struct* 1282:135259
- Sathya K, Nagarajan K, Carlin Geor Malar G, Rajalakshmi S, Raja Lakshmi P (2022) A comprehensive review on comparison among effluent treatment methods and modern methods of treatment of industrial wastewater effluent from different sources. *Appl Water Sci* 12(4):70. <https://doi.org/10.1007/s13201-022-01594-7>
- Sharma S, Bhattacharya A (2017) Drinking water contamination and treatment techniques. *Appl Water Sci* 7(3):1043–1067. <https://doi.org/10.1007/s13201-016-0455-7>
- Sheikh MC, Hasan MM, Hasan MN, Salman MS, Kubra KT, Awual ME (2023) Toxic cadmium (II) monitoring and removal from aqueous solution using ligand-based facial composite adsorbent. *J Mol Liq* 389:122854
- Sikosana ML, Sikhwivhilu K, Moutloali R, Madyira DM (2019) Municipal wastewater treatment technologies: a review. *Procedia Manuf* 35:1018–1024. <https://doi.org/10.1016/j.promfg.2019.06.051>
- Sitko R, Musielak M, Serda M, Talik E, Zawisza B, Gagor A (2021) Thiosemicarbazide-grafted graphene oxide as superior adsorbent for highly efficient and selective removal of mercury ions from water. *Sep Purif Technol* 254:117606
- Sultana M, Rownok MH, Sabrin M, Rahaman MH, Alam SMN (2022) A review on experimental chemically modified activated carbon to enhance dye and heavy metals adsorption. *Clean Eng Technol* 6:100382. <https://doi.org/10.1016/j.clet.2021.100382>
- Sun Q, Wang L, Li Y, Li L, Li S, Zhu G (2023a) Highly efficient removal of mercury ions from aqueous solutions by thiol-functionalized graphene oxide. *Water* 15(14):2529
- Sun T, Sun Y, Xu Y, Wang L, Liang X (2023b) Effective removal of Hg²⁺ and Cd²⁺ in aqueous systems by Fe–Mn oxide modified biochar: a combined experimental and DFT calculation. *Desalination* 549:116306
- Tene T, Arias Arias F, Guevara M, Nuñez A, Villamagua L, Tapia C (2022) Removal of mercury(II) from aqueous solution by partially reduced graphene oxide. *Sci Rep* 12(1):6326. <https://doi.org/10.1038/s41598-022-10259-z>
- Tran M-H, Booth I, Azarakhshi A, Berrang P, Wulff J, Brolo AG (2023) Synthesis of graphene and graphene films with minimal structural defects. *ACS Omega* 8(43):40387–40395. <https://doi.org/10.1021/acsomega.3c04788>
- Vardhan KH, Kumar PS, Panda RC (2019) A review on heavy metal pollution, toxicity and remedial measures: current trends and future perspectives. *J Mol Liq* 290:111197. <https://doi.org/10.1016/j.molliq.2019.111197>
- Vedenyapina M, Kurmysheva A, Kulaishin S, Kryazhev Y (2021) Adsorption of heavy metals on activated carbons (a review). *Solid Fuel Chem* 55:83–104. <https://doi.org/10.3103/S0361521921020099>
- Velarde L, Nabavi M, Escalera E, Antti M-L, Akhtar F (2023) Adsorption of heavy metals on natural zeolites: a review. *Chemosphere* 328:138508. <https://doi.org/10.1016/j.chemosphere.2023.138508>
- Vicente-Martínez Y, Caravaca M, Soto-Meca A, De Francisco-Ortiz O, Gimeno F (2020) Graphene oxide and graphene oxide functionalized with silver nanoparticles as adsorbents of phosphates in waters. A comparative study. *Sci Total Environ* 709:136111. <https://doi.org/10.1016/j.scitotenv.2019.136111>
- Waly SM, El-Wakil AM, Abou El-Maaty WM, Awad FS (2021) Efficient removal of Pb (II) and Hg (II) ions from aqueous solution by amine and thiol modified activated carbon. *J Saudi Chem Soc* 25(8):101296
- Wang J, Guo X (2020) Adsorption kinetic models: physical meanings, applications, and solving methods. *J Hazard Mater* 390:122156. <https://doi.org/10.1016/j.jhazmat.2020.122156>
- Yang X, Zhou B, Wang C, Tan R, Cheng S, Saleem A (2023) Mesoporous silica nanoparticles for the uptake of toxic antimony from aqueous matrices. *ACS Omega* 8(30):26916–26925. <https://doi.org/10.1021/acsomega.3c01735>
- Yap PL, Tung TT, Kabiri S, Matulick N, Tran DN, Losic D (2020) Polyamine-modified reduced graphene oxide: a new and cost-effective adsorbent for efficient removal of mercury in waters. *Sep Purif Technol* 238:116441

- Yu W, Sisi L, Haiyan Y, Jie L (2020) Progress in the functional modification of graphene/graphene oxide: a review. *RSC Adv* 10(26):15328–15345. <https://doi.org/10.1039/D0RA01068E>
- Yuan Y, An Z, Zhang R, Wei X, Lai B (2021) Efficiencies and mechanisms of heavy metals adsorption on waste leather-derived high-nitrogen activated carbon. *J Clean Prod* 293:126215. <https://doi.org/10.1016/j.jclepro.2021.126215>

Publisher's Note Springer Nature remains neutral with regard to jurisdictional claims in published maps and institutional affiliations.